Electronic Supplementary Material (ESI) for Journal of Materials Chemistry A.

Supporting Information

Fabrication of Freestanding Metal Organic Framework Predominant Hollow Fiber Mat and Its Potential Applications in Gas Separation and Catalysis

Zijian Dai [a,b], *Dennis T. Lee* [b], *Kaihang Shi* [b], *Siyao Wang* [b], *Heather F. Barton* [b], *Jie Zhu* [c], *Jiaqi Yan* [b], *Qinfei Ke* [a,*], *and Gregory N. Parsons* [b,*]

a Key Laboratory of Textile Science & Technology, Ministry of Education, College of Textiles, Donghua University, Shanghai, 201620, China

b Department of Chemical & Biomolecular Engineering, North Carolina State University, 911 Partners Way, Raleigh, North Carolina 27695, United States

c School of Fashion Engineering, Shanghai University of Engineering Science, No.333 Longteng Road, Songjiang, Shanghai, 201620, China

Section 1-Materials and Synthesis

1. Materials

Cellulose diacetate (CDA, Eastman Chemicals), diethyl zinc (DEZ, 95% STREM Chemicals Inc.,), trimethyl aluminum (TMA, 98% STREM Chemicals Inc.,), 2-amino-terephthalic acid (99%, Acros Organics), aluminum chloride hexahydrate ($AlCl_3 \cdot 6H_2O$, Alfa Aesar), copper nitrate trihydrate ($Cu(NO_3)_2 \cdot 3H_2O$, 99-104%, Sigma-Aldrich), 2-methylimidazole (99%, Sigma-Aldrich), meso-Tetra (4-carboxyphenyl) porphine (H_2TCPP, >97% Frontier Scientific), acetone (Fisher), N,N-dimethylformamide (DMF, Fisher), N,N-dimethylacetamide (DMAc, 99.8%, Sigma-Aldrich), anhydrous ethanol (200 proof, VWR), were purchased from commercial sources and used without further treatment. Melt-blown polypropylene (PP) fiber mats with density of 40 gsm was used as received from Nonwovens Cooperative Research Center (NCRC), North Carolina State University.

2. Fabrication of Cellulose Diacetate Nanofiber Mats

CDA nanofiber mats were fabricated by electrospinning technique. The electrospinning system used in this experiment consisted of a high voltage power supply (Precision Inc.,), a syringe pump (New Era Pump System Inc.,) and a conductive collector. Briefly, CDA was dissolved overnight in acetone/DMAc (2:1, v/v) to reach a CDA final concentration of 11 wt%. The polymer solution was then loaded into a plastic syringe with a 27 gauge stainless needle. The feed rate of 0.5 mL h^{-1} and a 13 kV voltage were controlled. The collection distance was fixed at 15 cm and the as-spun CDA nanofiber mats were collected on the metallic collector covered with aluminum foil. Electrospinning was performed at ambient temperature and the relative humidity was maintained at around 60%.

3. Atomic Layer Deposition of Al_2O_3 and ZnO on CDA Nanofiber Mats

CDA nanofiber mats were conformally coated with Al_2O_3 and ZnO thin films using a homebuilt hot-wall viscous-flow ALD reactor as previous work described[1]. ALD deposition with the metal oxide of Al_2O_3 and ZnO was both conducted at 90 °C under ~1.8 Torr. In a typical ALD Al_2O_3 cycle, TMA was first dosed to the reactor chamber for 2 s, followed by N_2 purge for 40 s. After another 2 s of H_2O dosing, the chamber was swept by N_2 for 60 s to complete one ALD running cycle. While in ALD ZnO process, the dose time of the DEZ precursors was set to 2s with a different interval of N_2 purge of 60 s. These as-prepared samples were referred as CDA@Al_2O_3 and CDA@ZnO, respectively.

4. Synthesis of MIL-53(Al)-NH_2 Powder

MIL-53(Al)-NH_2 powders were synthesized adapting from previous reports[2]. $AlCl_3 \cdot 6H_2O$ (0.966 g) was picked up as metal source, mixed with 2-amino-terephthalic acid (0.725 g) dissolved in 20 mL co-solvent mix solution (DMF/Water = 3/1, v/v) which is derived after the pre-experiments. The mixture was then transferred into a 100 mL Telfon-lined stainless-steel autoclave reactor and heated at 150 °C for 24 h. After cooling, the MIL-53(Al)-NH_2 product was washed twice by hot DMF for 24 h to remove unreacted 2-amino-terephthalic acid linkers and collected by filtration. After that, the powders were washed by anhydrous ethanol for another two times to remove DMF. The resulting materials were finally dried and burned under vacuum at 200 °C for 10 h.

5. Synthesis of MIL-53(Al)-NH_2 Predominant Hollow Fiber Mats

To synthesize MIL-53(Al)-NH_2 predominant hollow fiber mats, the CDA@Al_2O_3 nanofiber mat was first immersed in acetone and heated up to 120 °C for 24 h to dissolve and remove out the CDA polymers. After the delicate treatment, the majority of CDA polymers (~ 90%) were removed out from the CDA@Al_2O_3 nanofiber mats, left with an Al_2O_3 hollow fiber mats with tiny polymer residuals. For the conversion of MIL-53(Al)-NH_2 using Al_2O_3 hollow fiber mats as the metal source, 0.106 g 2-amino-terephthalic acid was firstly added to a 20 mL DMF/ water mixture (3/1, v/v), then the mixture was sonicated and stirred for 20 min until complete dissolution. Subsequently, a piece of Al_2O_3 hollow fiber mat (0.030 g) was gently soaked in the prepared solution and transferred into a 100 mL Telfon-lined stainless-steel autoclave reactor. This reactor was then heated at 120 ^{o}C for 20 h to finish the solvothermal synthesis. After complete reaction, the as-received MIL-53(Al)-NH_2 hollow fiber mat was washed twice with hot DMF, followed by another 2 times of anhydrous ethanol washing. The MIL-53(Al)-NH_2 hollow fiber mat was finally dried under vacuum at 200 ^{o}C for 10 h and stored in a desiccator before test. As a control group, CDA@Al_2O_3 nanofiber mat was also converted into MIL-53(Al)-NH_2 directly using the same recipe mentioned above without the pretreatment in acetone solution. The as-prepared sample was denoted as MIL-53(Al)-NH_2 (CDA).

6. Synthesis of MIL-53(Al)-NH_2 onto PP Nonwovens

0.062 g 2-amino-terephthalic acid was dispersed in 20 mL DMF/ water mixtures (3/1, v/v) in 100 mL Telfon-lined stainless-steel autoclave reactor. Subsequently, melt-blown PP fiber mats (1" × 2") coated with 200 cycles of ALD Al_2O_3 (PP@Al_2O_3) were added into the solution. The autoclave was transferred into an oven and heated to 120 ^{o}C for 20 h. After the reaction done, the MIL-53(Al)-NH_2 (PP) swatch was washed twice with hot DMF and rinsed with anhydrous ethanol 2 times. The resulting MIL-53(Al)-NH_2 (PP) swatch was dried under vacuum at 120 ^{o}C for 12 h and stored in a desiccator before other measurements.

7. Synthesis of ZIF-8 Predominant Hollow Fiber Mats

To synthesize ZIF-8 predominant hollow fiber mat, 0.10 g 2-methylimidazole was dispersed into 20 mL DMF. ZnO hollow fiber mat (obtained from dissolving CDA@ZnO into acetone, 0.03g) was subsequently soaked in the solution. The as-prepared precursor mixture was then transferred into a 100 mL Telfon-lined stainless-steel autoclave reactor and heated to 100 ^{o}C for 10 h. After the reaction done, the as-received ZIF-8 hollow fiber mat was washed twice with hot DMF, followed by another 2 times of anhydrous ethanol washing. The ZIF-8 hollow fiber mat was finally dried under vacuum at 100 ^{o}C for 10 h and stored in a desiccator before test.

8. Synthesis of Al-TCPP predominant hollow fiber mats

0.23 g H_2TCPP was dissolved in a DMF (5mL) and water mixture (15mL). Subsequently, Al_2O_3 hollow fiber mat (0.03 g) was fully immersed in the solution mixture. The as-prepared precursor mixture was then transferred into a 100 mL Telfon-lined stainless-steel autoclave reactor and heated to 120 ^{o}C for 20 h. After the reaction done, the as-received Al-TCPP hollow fiber mat was washed twice with hot DMF, followed by another 2 times of anhydrous ethanol washing. The Al-TCPP hollow fiber mat was finally dried under vacuum at 100 ^{o}C for 10 h and stored in a desiccator before test.

Section 2-Characterization

1. Scanning electron microscopic (SEM) and X-ray photoelectron spectroscopy (XPS)

SEM was conducted using a FEI Verios 460 L field emission SEM. X-ray diffraction (XRD) was taken with a Rigaku SmartLab X-ray diffraction tool (Cu Kα X-ray source) for crystalline structure characterization. XPS was performed on a Kratos Analytical Axis Ultra system equipped with aluminum gun (Al Kα = 1486.6 eV radiation). Voltage and current of x-ray gun was 15 kV and 20 mA. All the binding energies were calibrated using contaminated carbon (C1s = 284.6 eV).

2. Thermogravimetric Analysis and CO_2 Cycling Measurement

CO_2 cycling experiments were carried out on a TA instruments SDT 650. 15% CO_2/N_2 (Acro) and N_2 (99.999%) were used in this experiment. In a typical test, ~10 mg target sample was loaded into an alumina pan, with a flow rate of 100 mL/min for both gases. The sample was first heated at 100 ^oC for 40 min under N_2 atmosphere to complete degassing, after the temperature was cooling down to 25 ^oC, MOF sample was swept continuously by CO_2 for 20 min, and then flowing N_2 was maintained for 40 min at 100 ^oC for activating MOF sample in every cycle.

3. Adsorption and Catalytic Activity Test

The HCHO adsorption and catalytic activities were evaluated in static state which was adapted from previous reports[3]. A polytetrafluoroethylene layer stainless steel reactor (0.5 L) was used, at the bottom of which was placed a quartz Petri dish with swatch inside. After putting the dish into the reactor, 300 ppm of HCHO which was generated from S-4000 Gas Mixing system (Environics, USA) was injected into the reactor. After stabilizing the concentration of HCHO to 150 ppm, the cover of the dish was removed to start the adsorption and catalytic reaction of HCHO. HCHO, CO_2, CO and water vapor were recorded online by a photoacoustic IR multigas monitor (INNOVA AirTech Instruments Model 1412i) during test at 25 °C. The yield of CO_2 (ΔCO_2) and the concentration variation of HCHO were calculated to analyze the HCHO removal ratio.

Section 3-Calculation of MOF Conversion Ratio

General

The conversion ratio of MOFs based on ALD precursors was calculated by adapting equations first published by Bechelany's group.

Equation

x = quantity (mol) of metal in the oxide

y = quantity (mol) of metal in the MOF

A = total quantity (mol) of metal in the MOF hollow fiber mats

B = final weight of the MOF hollow fiber mats

$M_W x$ = oxide molecular weight (g/mol)

$M_W y$ = MOF molecular weight (g/mol)

As far as the metal loss was not detected during the synthesis, A was considered as a constant:

$$A = x + y \tag{S1}$$

The final weight of the MOF hollow fiber mats is written as (Al_2O_3 is chosen as metal source):

$$B = \frac{X}{2} \times M_W x + y \times M_W y \tag{S2}$$

By replacing (x = A-y) in (S2), y can be calculated by:

$$y = (2B - A \times M_W x) \div (2M_W y - M_W x) \tag{S3}$$

The conversion ratio can thus be written as follows:

$$Conversion\ ratio = 100 \times (y \div A) = 100 \times [(2B - A \times M_W x) \div (2M_W y - M_W x)] \div A \tag{S4}$$

Section 4-Results

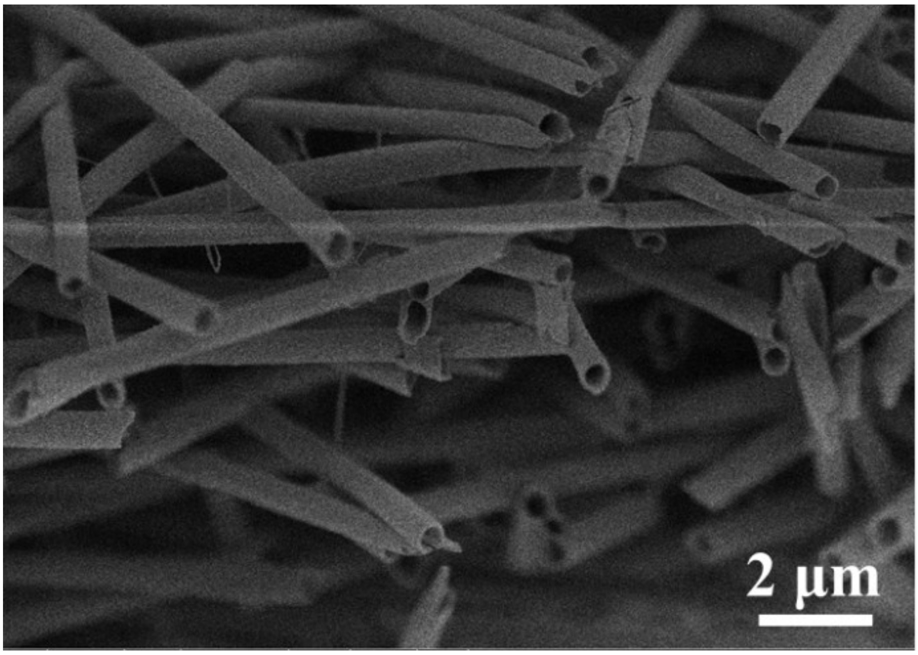

Figure S1. Cross-sectional SEM image of hollow Al_2O_3 fiber mat.

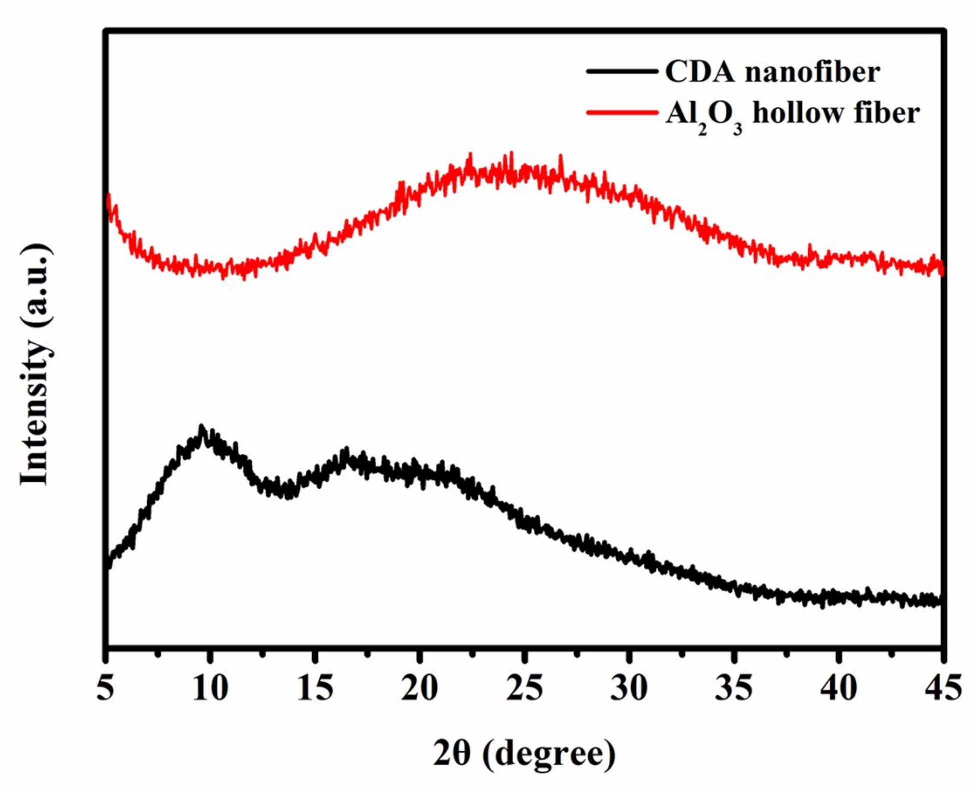

Figure S2. XRD pattern of pristine CDA nanofiber and Al_2O_3 hollow fiber mat obtained from rising Al_2O_3/CDA in acetone at 120 ^{o}C for 12 h.

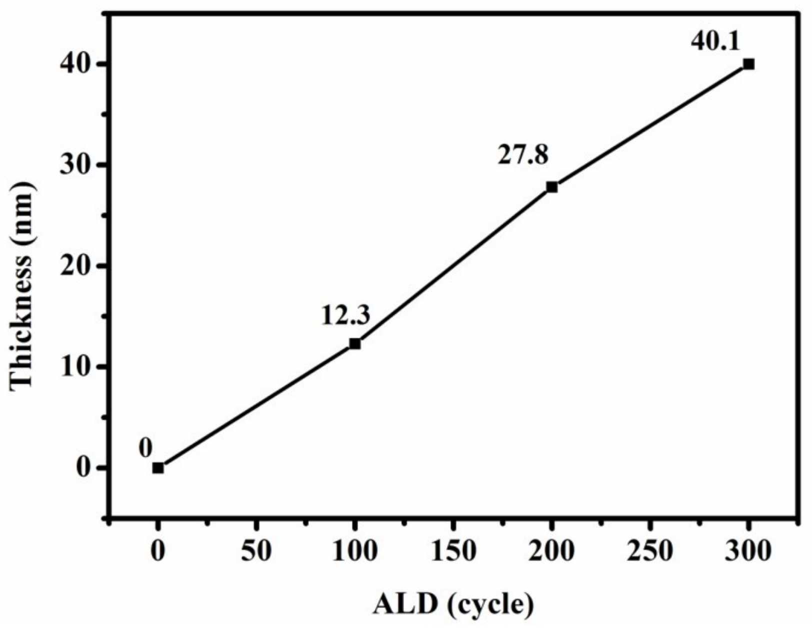

Figure S3. Al_2O_3 real thickness as a function of running cycles.

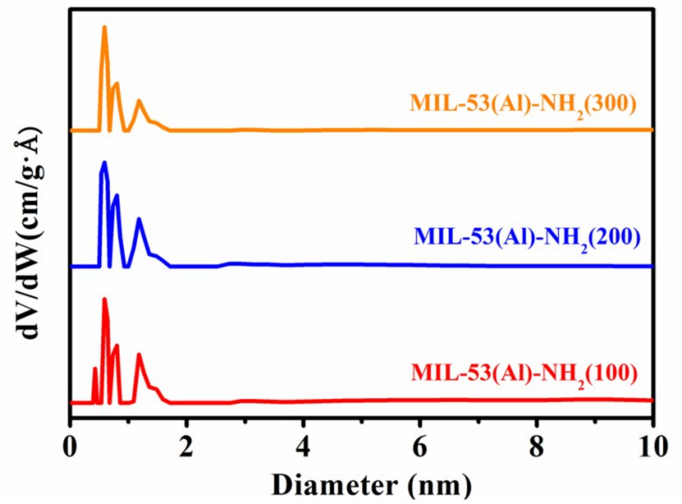

Figure S4. Pore size distribution curves: DFT at 77 K of MIL-53(Al)-NH$_2$ (100), MIL-53(Al)-NH$_2$ (200), and MIL-53(Al)-NH$_2$ (300).

Figure S5. Optical photographs of (a) MIL-53(Al)-NH$_2$ (100), (b) MIL-53(Al)-NH$_2$ (200), and (c) MIL-53(Al)-NH$_2$ (300).

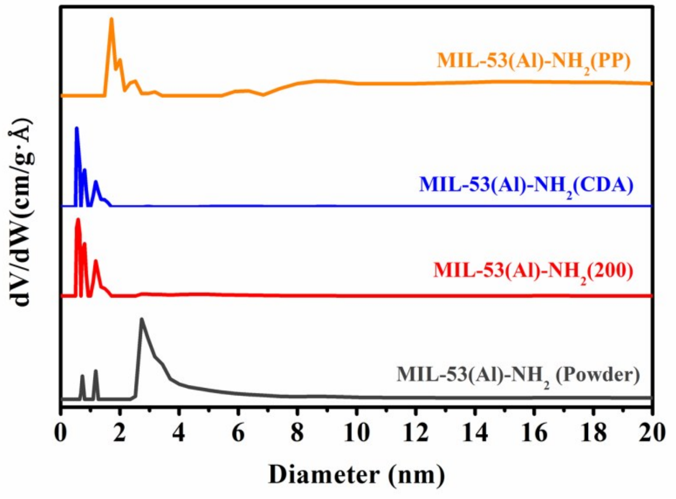

Figure S6. Pore size distribution curves: DFT at 77 K of MIL-53(Al)-NH$_2$ (powder), MIL-53(Al)-NH$_2$ (200), MIL-53(Al)-NH$_2$ (CDA) and MIL-53(Al)-NH$_2$ (PP).

Table S1. Physical parameters and CO_2 adsorption uptake in selected MIL-53(Al)-NH_2

MOF	Surface areas S_{BET} (m^2 g^{-1})	Pore volume V_p (cm^3 g^{-1})	Conversion ratio (%)	CO_2 adsorption capacity (mmol g^{-1})			$S_{CO2/N2}$ [a]	Ref
				bar	273 K	298K		
MIL-53(Al)-NH_2 (100)	880 ± 30	0.76	100	1	3.91 ± 0.1	1.81	-	This work
MIL-53(Al)-NH_2 (200)	842 ± 28	0.65	97	1	3.30 ± 0.05	1.65		This work
MIL-53(Al)-NH_2 (300)	720 ± 40	0.50	74	1	2.65 ± 0.08	1.45	-	This work
MIL-53(Al)-NH_2 (powder)	1089 ± 112	0.62	-	1	2.35 ± 0.11	2.16		This work
MIL-53(Al)-NH_2 (CDA)	480 ± 21	0.28	-	1	1.98 ± 0.13	1.29		This work
MIL-53(Al)-NH_2 (PP)	3.55 ± 2.7	0.009	-	1	0.17 ± 0.01	0.10		This work
MIL-53-NH_2 (membrane)	-	-	-	1	3.09	2.14	-	[4]
MIL-53-NH_2 (powder)	-	-	-	1	2.24	-	-	[5]
MIL-53 (powder)	905	0.40	-	-	-	-		[6]
MIL-53-NH_2 (powder)	400	1.03	-	1	2.18	1.88	42.3	[7]

a IAST selectivity based on a gas mixture of 0.15 bar N_2 and 0.85 bar CO_2

Section 5- Experimental and Simulated Sorption Studies

1. Low-pressure Gas Adsorption Measurements.

Gas adsorption isotherms in the pressure range of 0-1.1 bar were measured by a volumetric method using a Micromeritics 3Flex Surface Characterization Analyzer. Before analysis, all samples were fully degassed under vacuum at 120 ^{o}C for 20 h. After the degas process is completed, the sample tubes were weighted and then carefully transferred to the analysis port of the gas adsorption instrument. N_2 adsorption-desorption isotherms at 77 K were measured in liquid nitrogen. N_2 and CO_2 adsorption-desorption isotherms at 273 K were measured using an ice water bath and isotherms at 298 K were measured using water baths. All temperatures were monitored before and after the measurement and no temperature change had been detected in all cases.

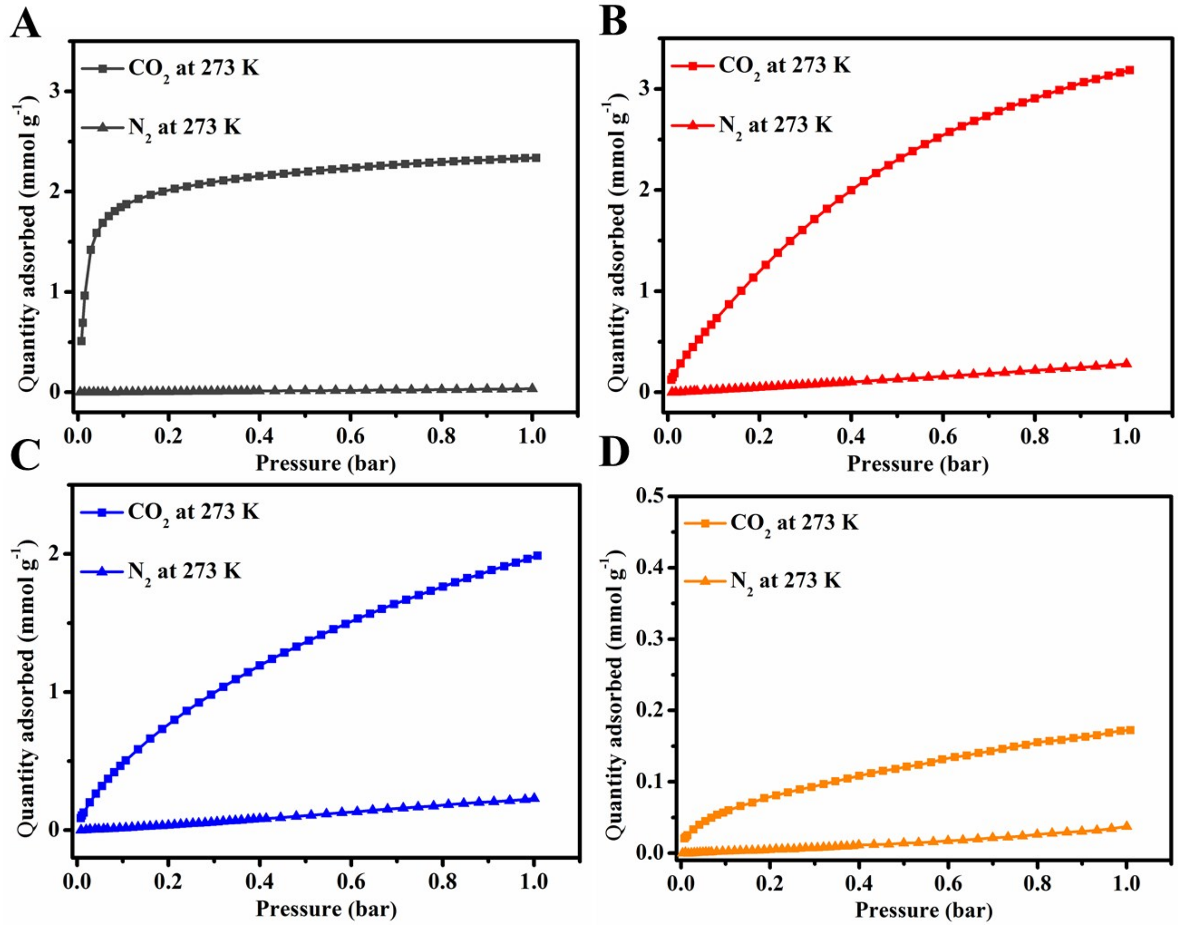

Figure S7. Single component of CO_2 and N_2 adsorption isotherms of (A) MIL-53(Al)-NH_2 (powder), (B) MIL-53(Al)-NH_2 (200), (C) MIL-53(Al)-NH_2 (CDA), and MIL-53(Al)-NH_2 (PP) at 273 K.

3. Isotherms from IAST simulations and CO_2/N_2 selectivity

Calculation details

To predict CO_2/N_2 selectivity, we applied the ideal adsorbed solution theory (IAST)[8]. The IAST can predict a mixed-gas adsorption based on the experimental pure isotherm data and requires no data for the mixture. The IAST relates the adsorbed phase and the gas phase using the general thermodynamic equations by assuming an ideal gas phase (which is an excellent approximation for pressure less than 1 atm) and an ideal solution for the adsorbed phase (i.e., activity coefficient is unity). An expression analogous to the Raoult's law can be obtained,

$$Py_i = P_i^0 x_i \tag{S5}$$

where P is the total pressure in the gas phase; y_i is the mole fraction of component *i* in the gas phase; P_i^0 is the pure vapor pressure for component *i* at the temperature T and the spreading pressure π of the adsorbed mixture; and x_i is the mole fraction of component *i* in the adsorbed mixture. In practice, the total pressure P and the mole fraction of each component y_i in the binary-gas phase are usually given, to determine the unknown variables P_i^0 and x_i, we need to resort to the Gibbs adsorption isotherm to calculate the spreading pressure π,

$$\frac{A\pi}{RT} = \int_0^{P_1^0} \frac{n_1(p)}{p} dp = \int_0^{P_2^0} \frac{n_2(p)}{p} dp \tag{S6}$$

where A is the surface area of adsorbent and R is the gas constant; $n_i(p)$ is the experimental isotherm data for pure component *i* and is a function of pressure, we use lower case p here to indicate that it's a dummy integral variable. The integration in Eq. (S6) needs to be carried out up to a pressure that is usually higher than the experimental pressure limit (1 bar) accessible to the normal vapor sorption analyzer. Thus, fitting the current experimental isotherm data to an adsorption model is required and the isotherm data at any pressure can then be predicted by the fitted equation. The IAST doesn't specify the fitting model for the pure isotherm, any adsorption model could be potentially used here. In this work, we found the Sips equation 9 fits the experimental pure adsorption isotherm data better than the Toth [11] and Langmuir equations 10, so we applied the Sips equation here,

$$n_i = n_s \frac{(bP)^{1/n}}{1+(bP)^{1/n}} \tag{S7}$$

where n_s, b and n are the saturation adsorption capacity, adsorption equilibrium constant and the parameter characterizing the system heterogeneity, respectively. The heterogeneity of the system may result from the adsorbent or adsorbate or the combination of both [11]; the larger the value n is, the more heterogeneous the system is. The parameter n is temperature dependent, and its value would decrease with the temperature [11]. When $n = 1$, Equation. S7 reduces to the Langmuir equation assuming the adsorption on a homogeneous flat surface. Such behavior of the parameter n with the temperature is consistent with the statistical mechanical analysis of the adsorption on heterogeneous surfaces [12, 13].

Now, we have a well-posed math problem, we have four equations (two of Equation S5 for each component, Equation S6 and remembering $x_1 + x_2 = 1$), and four unknown variables (P_i^0 and x_i for each component in a binary mixture). Once we obtain the mole fraction x_i in the adsorbed phase, we can determine the total adsorbed amount based on the fact that there is no molecular area change upon mixing in the ideal adsorbed solution,

$$\frac{1}{n_t} = \frac{x_1}{n_1^0} + \frac{x_2}{n_2^0} \tag{S8}$$

where n_t is the total adsorbed amount for the mixture; n_1^0 and n_2^0 are the adsorbed amount for the pure component at temperature T and gas-phase pressure P_1^0 and P_2^0, respectively, and they can be obtained either from experiments or fitted equations [e.g., Equation S7]. The MATLAB code for the IAST calculations has been validated against the reported data [11] and is available on https://github.com/KaihangShi/IAST. The selectivity coefficient has been defined as[8]

$$S = \frac{x_1/x_2}{y_1/y_2} \tag{S9}$$

The quality of fit to the available experimental pure isotherm data is essential to the accuracy of the IAST calculation, and it has been emphasized a lot in real applications[14]. The possible dependence of fitting parameters on the initial guess and constraint bound of the fitting algorithm, however, is generally overlooked, which is especially important for the less-adsorbed component not showing much curvature in its isotherm data. An example is shown in **Figure** S8 where two equations both fit experimental data very well but showing distinct shape at high pressure region. If possible, the experimental isotherm data at high pressure should be collected to reduce the uncertainty in the fitting process.

Here, we fit our pure adsorption isotherm data for CO_2 and N_2 by choosing different initial guesses of the fitting parameters and setting lower bound of those parameters to 0. For CO_2 adsorption in a specific sample at 273 K, the final Sips equation is generally fixed; while for N_2, because its adsorption isotherm doesn't show enough curvature, the corresponding fitting parameters exhibit high variance (**Figure S8**). We tentatively chose two cases with a low saturation capacity, n_s, and a high saturation capacity, and to see how this difference will affect the final IAST selectivity. Fitting parameters are tabulated in **Table S2**.

For adsorption in powder, as expected, the selectivity strongly depends on the fitting equation of the less-adsorbed N_2 because in this case we have to integrate the isotherm data up to an extremely high pressure [Equation S6]. When using the fitting equation with a high saturation capacity for N_2, the selectivity at 1 bar is 1637 and 1800 for 50/50 and 15/85 CO_2/N_2, respectively (**Figure** S11). If the fitting equation with a low saturation capacity is used for N_2, the selectivity will blow up and reaches $1.85*10^8$ and $2.19*10^6$ for 50/50 and 15/85 CO_2/N_2, respectively.

For adsorption in MIL-53(Al)-NH_2-200/CDA/PP case, the selectivity shows weak dependence on the different fitting equations for N_2 used. At 1 bar, MIL-53(Al)-NH_2 (200) has the highest selectivity amount three samples.

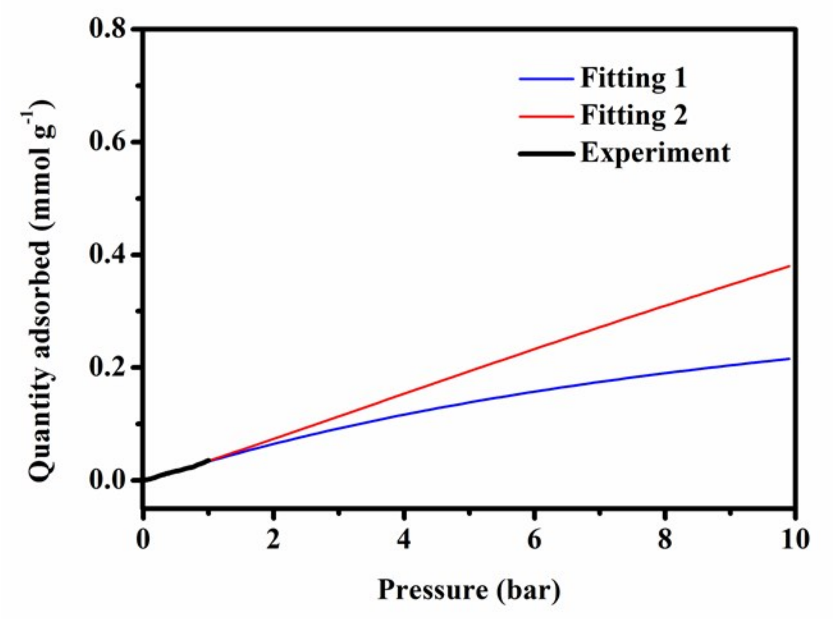

Figure S8. N_2 adsorption isotherms in MIL-53(Al)-NH_2 (powder) at 273 K.

Table S2. Fitting parameters of Sips model to pure adsorption isotherms at 273 K. For N_2 case, we chose two fitting equations that both fit experimental data well but with a low and a high saturation capacity, n_s.

Sample	Gas	n_s [mmol/g]	b [1/kPa]	n	R-square
Powder	CO_2	2.331	0.4229	1.039	0.9866
	N_2	0.4524 2.489	0.000922 0.0002161	0.9408 0.8989	0.9953 0.995
MIL-53-NH_2 (200)	CO_2	5.53	0.01368	1.012	0.9995
	N_2	3.726 9.427	0.001091 0.0004129	0.8769 0.9096	0.9998 0.9998
MIL-53-NH_2 (CDA)	CO_2	6.299	0.003601	1.305	1.0
	N_2	7.828 20.13	0.0003587 0.0001337	0.9388 0.9567	0.9986 0.9984
MIL-53-NH_2 (PP)	CO_2	3.801	7.309e-05	1.59	0.9973
	N_2	0.2742 0.8652	0.002186 0.0009088	0.7747 0.7573	0.9931 0.9959

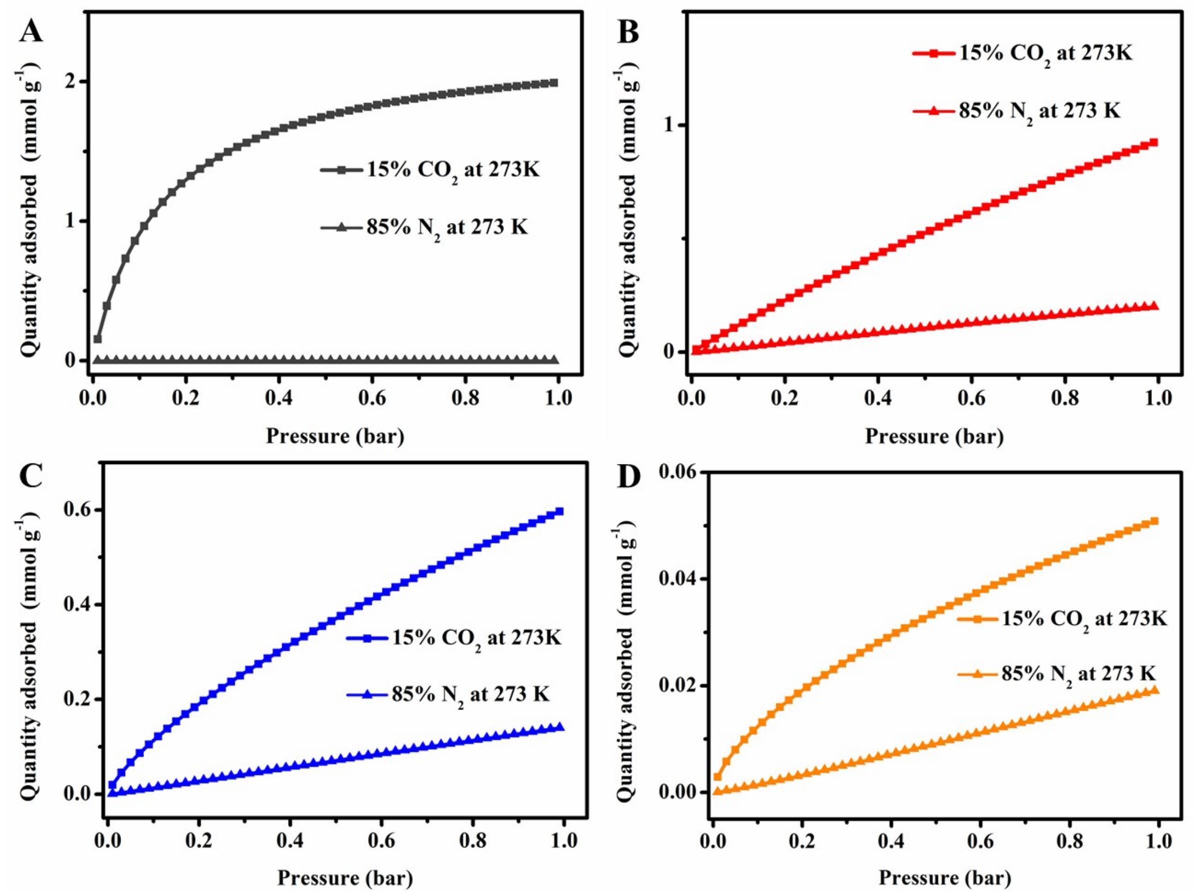

Figure S9. IAST binary adsorption isotherms for (A) MIL-53(Al)-NH_2 (powder), (B) MIL-53(Al)-NH_2 (200), (C) MIL-53(Al)-NH_2 (CDA), and (D) MIL-53(Al)-NH_2 (PP) at 273 K with CO_2 and N_2 molar ratio of 15/85 in the gas phase.

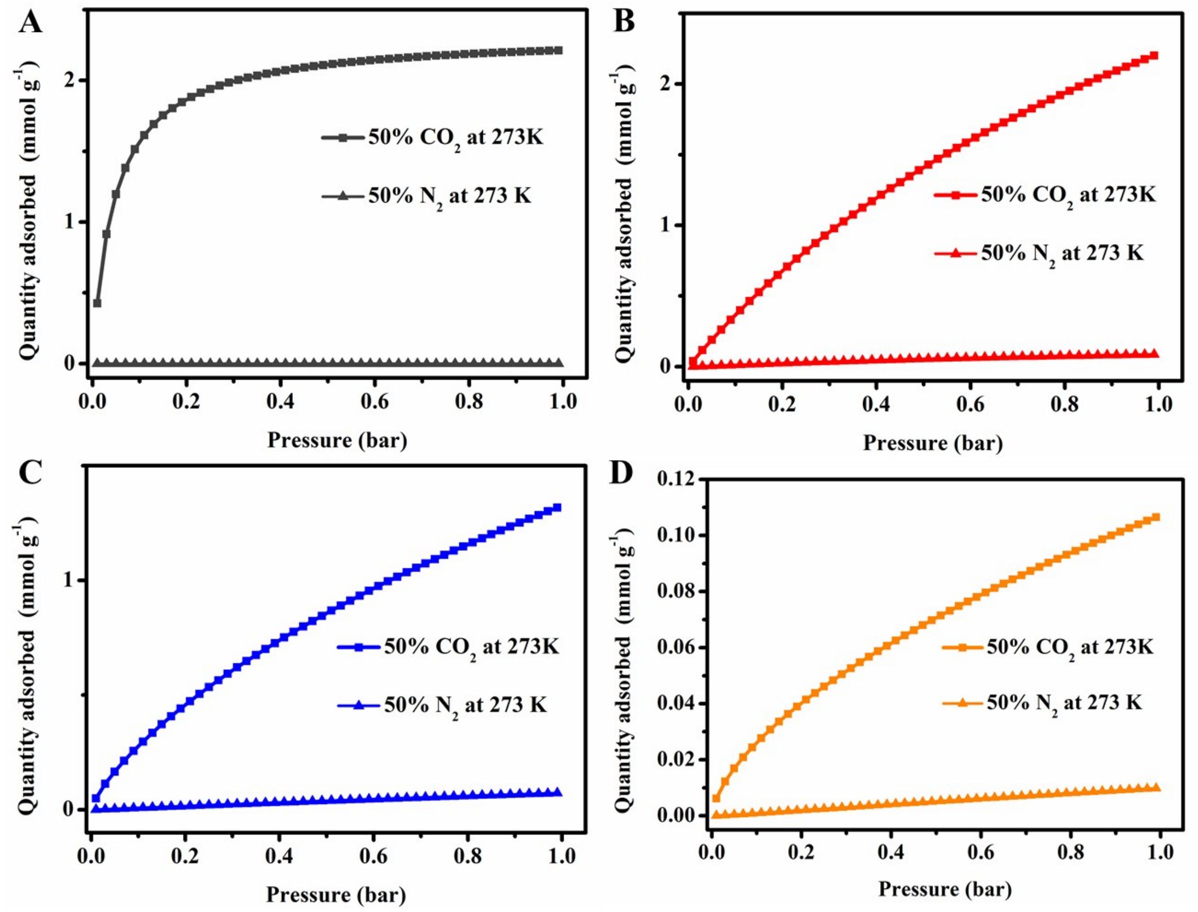

Figure S10. IAST binary adsorption isotherms for (A) MIL-53(Al)-NH_2 (powder), (B) MIL-53(Al)-NH_2 (200), (C) MIL-53(Al)-NH_2 (CDA), and (D) MIL-53(Al)-NH_2 (PP) at 273 K with CO_2 and N_2 molar ratio of 50/50 in the gas phase.

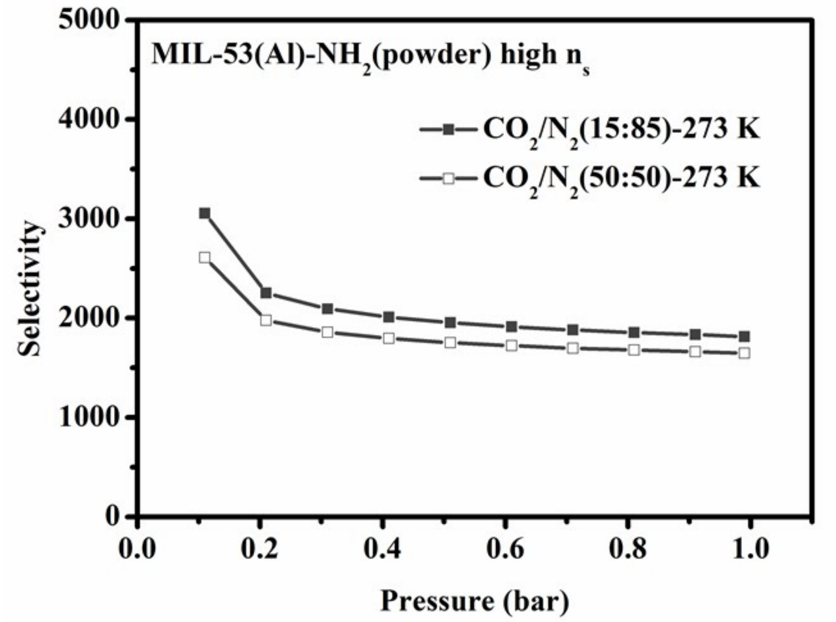

Figure S11. Selectivity by the IAST calculations for MIL-53(Al)-NH$_2$ (powder) at 273 K with CO$_2$ and N$_2$ molar ratio of 15/85 and 50/50 in the gas phase.

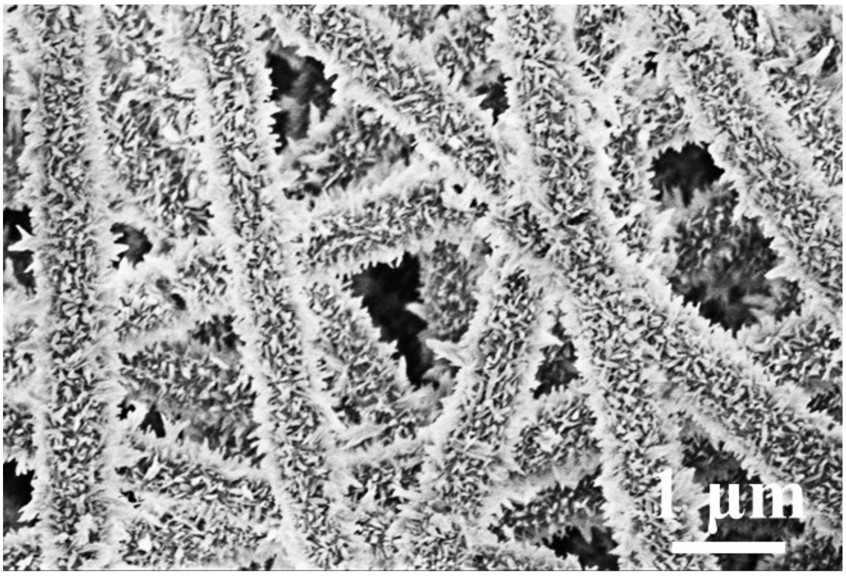

Figure S12. SEM image of MIL-53(Al)-NH$_2$ (200) after HCHO catalytic test.

Table S3. Summary of VOC removal performance over selected MOFs.

Material	Catalyst	VOCs	Test condition and Performance	Ref
MOF	P123/UiO-66	Toluene	Initial concentration: 1000 ppm; Adsorption capacity: 339 mg g^{-1}	15
MOF	Defective UiO-66	Toluene	Initial concentration: 1000 ppm; Adsorption capacity: 252 mg g^{-1}	16
MOF	Hydrophobic UiO-66	Toluene	Initial concentration: 1000 ppm; Adsorption capacity: 259 mg g^{-1}	17
MOF	Ga-MIL-53	Formaldehyde	Initial concentration: 2000 ppm Adsorption capacity: 70.0 mg g^{-1}	18
MOF	MOF-5	Formaldehyde	Initial concentration: 22.7 ppm Adsorption capacity: 0.11 mg g^{-1}	19
MOF	γ-CD-MOF-K	Formaldehyde	Initial concentration: 0.39 ppm Adsorption capacity: 36.7 mg g^{-1}	20
MOF	ZIF-67@PAN	Formaldehyde	Initial concentration: 0.35 ppm Removal efficiency: 84 %	21
MOF	MIL-101	Formaldehyde	Initial concentration: 150 ppm Adsorption capacity: 164.8 mg g^{-1}	22
MOF	MIL-53(Al)-NH_2 (200)	Formaldehyde	Initial concentration: 150 ppm Removal efficiency: 100 %	This work

Reference

1. J. J. Zhao, B. Gong, W. T. Nunn, P. C. Lemaire, E. C. Stevens, F. I. Sidi, P. S. Williams, C. J. Oldham, H. J. Walls, S. D. Shepherd, M. A. Browe, G. W. Peterson, M. D. Losego and G. N. Parsons, *Journal of Materials Chemistry A*, 2015, **3**, 1458-1464.
2. L. Bolinois, T. Kundu, X. R. Wang, Y. X. Wang, Z. G. Hu, K. Koh and D. Zhao, *Chemical Communications*, 2017, **53**, 8118-8121.
3. Z. J. Dai, X. W. Yu, C. Huang, M. Li, J. F. Su, Y. P. Guo, H. Xu and Q. F. Ke, *RSC Advances*, 2016, **6**, 97022-97029.
4. F. Zhang, X. Q. Zou, X. Gao, S. J. Fan, F. X. Sun, H. Ren and G. S. Zhu, *Advanced Functional Materials*, 2012, **22**, 3583-3590.
5. P. Serra-Crespo, E. Gobechiya, E. V. Ramos-Fernandez, J. Juan-Alcaniz, A. Martinez-Joaristi, E. Stavitski, C. E. A. Kirschhock, J. A. Martens, F. Kapteijn and J. Gascon, *Langmuir*, 2012, **28**, 12916-12922.
6. Z. H. Li, Y. N. Wu, J. Li, Y. M. Zhang, X. Zou and F. T. Li, *Chemistry-a European Journal*, 2015, **21**, 6913-6920.
7. H. R. Abid, Z. H. Rada, X. Duan, H. Sun and S. Wang, *Energy & Fuels*, 2018, **32**, 4502-4510.
8. A. L. Myers and J. M. Prausnitz, *Aiche Journal*, 1965, **11**, 121-+.
9. R. Sips, *Journal of Chemical Physics*, 1948, **16**, 490-495.
10. I. Langmuir, *Journal of the American Chemical Society*, 1918, **40**, 1361-1403.
11. N. Alvarez-Gutierrez, M. V. Gil, F. Rubiera and C. Pevida, *Fuel Processing Technology*, 2016, **142**, 361-369.
12. K. H. Shi, E. E. Santiso and K. E. Gubbins, *Langmuir*, 2019, **35**, 5975-5986.
13. E. Forte, A. J. Haslam, G. Jackson and E. A. Muller, *Physical Chemistry Chemical Physics*, 2014, **16**, 19165-

19180.

14. K. Sumida, D. L. Rogow, J. A. Mason, T. M. McDonald, E. D. Bloch, Z. R. Herm, T. H. Bae and J. R. Long, *Chemical Reviews*, 2012, **112**, 724-781.
15 X. D. Zhang, Y. Yang, X. T. Lv, Y. X. Wang, N. Liu, D. Chen and L. F. Cui, *Journal of Hazardous Materials*, 2019, **366**, 140-150.
16. X. D. Zhang, Y. Yang, L. Song, J. F. Chen, Y. Q. Yang and Y. X. Wang, *Journal of Hazardous Materials*, 2019, **365**, 597-605.
17. X. D. Zhang, X. T. Lv, X. Y. Shi, Y. Yang and Y. Q. Yang, *Journal of Colloid and Interface Science*, 2019, **539**, 152-160.
18. J.-P. Bellat, I. Bezverkhyy, G. Weber, S. Royer, R. Averlant, J.-M. Giraudon and J.-F. Lamonier, Journal of Hazardous Materials, 2015, **300**, 711-717.
19. Z.-Y. Gu, G. Wang and X.-P. Yan, *Analytical Chemistry*, 2010, **82**, 1365-1370.
20. L. Wang, X. Y. Liang, Z. Y. Chang, L. S. Ding, S. Zhang and B. J. Li, ACS Applied Materials & Interfaces, 2018, **10**, 42-46.
21. Y. Bian, R. T. Wang, S. J. Wang, C. Y. Yao, W. Ren, C. Chen and L. Zhang, *Journal of Materials Chemistry A*, 2018, **6**, 15807-15814.
22. Z. Wang, W. Z. Wang, D. Jiang, L. Zhang and Y. L. Zheng, *Dalton Transactions*, 2016, **45**, 11306-11311.